International Journal of Engineering & Technology, 7 (4.18) (2018) 277-282

International Journal of Engineering & Technology

Website: www.sciencepubco.com/index.php/IJET

Research paper

Fabrication of Nickel Oxide Nanowall Network Films at Different Annealing Temperatures for Humidity Sensing Applications

M.H. Mamat[1,2]*, N. Parimon[1], M.A.R. Abdullah[1], A.S. Ismail[1], M.F. Malek[2], W.R.W. Ahmad[1], A.S. Zoolfakar[1], A.B. Suriani[3], M.K. Ahmad[4], N. Nayan[4], I. B. Shameem Banu[5], R. Amiruddin[5], M. Rusop[1,2]

[1]NANO-ElecTronic Centre (NET), Faculty of Electrical Engineering, Universiti Teknologi MARA (UiTM), 40450 Shah Alam, Selangor, Malaysia
[2]NANO-SciTech Centre (NST), Institute of Science (IOS), Universiti Teknologi MARA (UiTM), 40450 Shah Alam, Selangor, Malaysia
[3]Nanotechnology Research Centre, Faculty of Science and Mathematics, Universiti Pendidikan Sultan Idris (UPSI), 35900 Tanjung Malim, Perak, Malaysia
[4]Microelectronic and Nanotechnology – Shamsuddin Research Centre (MiNT-SRC), Faculty of Electrical and Electronic Engineering, Universiti Tun Hussein Onn Malaysia (UTHM), Batu Pahat, Johor, Malaysia
[5]Department of Physics, B.S. Abdur Rahman Crescent Institute of Science & Technology, Vandalur, Chennai 600 048, India
**Corresponding author E-mail: mhmamat@salam.uitm.edu.my*

Abstract

Nickel oxide (NiO) nanowall network films were successfully prepared on indium tin oxide (ITO) glass substrates by sonicated sol-gel immersion method using a precursor solution of nickel nitrate hexahydrate. The NiO nanowall network films were annealed at different annealing temperature that ranges from 300 ^{0}C to 500 ^{0}C. The effects of annealing temperature on the structural, optical and humidity sensing properties of NiO nanowall network films were investigated by X-ray diffraction (XRD), field emission scanning electron microscopy (SEM), ultraviolet-visible (UV-vis) spectroscopy and humidity sensor measurement system. The X-ray diffraction patterns revealed that the grown NiO nanowall network films have a crystalline cubic structure. The UV-vis spectra demonstrates that the average transmittance value of all samples in the visible region are high and exceeded 90% transmission. The optical bandgap energy of NiO nanowall network films ranged from 3.76 to 3.77 eV. Results obtained showed that the humidity sensing performance of NiO nanowall network films are very promising and could be tuned by annealing temperatures.

Keywords: *nickel oxide; nanowall network film; structural properties; optical properties; humidity sensing.*

1. Introduction

Humidity sensors have received great attention in various fields including meteorology, chemical, agriculture, and medicine, which require the continuous monitoring of water vapour concentration. The humidity level is normally measured as relative humidity (RH), which defines as the pressure of actual vapour over the pressure of saturated vapour at a specified temperature. Among the desirable properties of humidity sensors are high sensitivity and reliability. Various materials have been explored for humidity sensor applications. These materials include polymer, photonic crystal, electrolytes, and metal oxides [1-5]. Particularly metal oxide-based humidity sensor, the performance of the device is very promising. Since the performance of the humidity sensor is closely related with availability of the surface area to react with water molecules, the metal oxide that has size in nano is favorable [6, 7]. The performance of sensors is also influenced by the morphology and structure of the metal oxide [8, 9]. Thus, the development of outstanding nanostructured metal oxide with good humidity sensing capability is very important to achieve high device performance.

Various metal oxides have shown great response to humidity such as zinc oxide (ZnO), tin oxide (SnO), titanium dioxide (TiO_2) and nickel oxide (NiO) [10-13]. NiO is one of the attractive materials with potential applications in solar cell, water splitting, and sensors [14-16]. NiO has p-type conductivity in native and it has structure similar with sodium chloride (NaCl). NiO can be fabricated by various physical and chemical approaches including sputtering, evaporation, chemical vapour deposition, and sol-gel [17-23]. Particularly in nanowall network configuration, the humidity response using NiO film is expectedly to enhance due to high surface area availibity and porous surface. The three-dimensional mesoporous nanowall with well-connected structure also offers a numerous active sites on the exposed surface for humidity sensing applications. There are several techniques used to enhance the surface properties of NiO nanostructures. Among them are doping process, metal-coating, and heat treatment [24-26]. Among these approaches, tailoring of NiO nanostructures by heat treatment presents a facile and good potential for tuning the response and sensitivity during humidity sensing.

Accordingly, NiO nanowall network films with different annealing temperatures were prepared in the present study and their humidity sensing properties were investigated. The nanowall

network films were grown using a facile route of sol-gel immersion method at temperature of 70^{0}C. The main focus of this research was the finding of appropriate annealing temperature for designing highly responsive NiO nanowall network films with high sensitivity and stability.

2. Experimental Procedure

In this work, an indium tin oxide (ITO)-coated glass was used as a substrate to grow NiO nanowall arrays. Prior to the growth process, ITO glass was cleaned using solutions of acetone, methanol and de-ionized (DI) water in the ultrasonic bath (Hwasin Technology PowerSonic 405, 40k Hz) for 10 min each. Next, the ITO glass was dried using nitrogen gas. To grow NiO nanowall network films, a solution consisting of 0.1M nickel (II) nitrate hexahydrate and 0.1M hexamethylenetetramine (HMT) was prepared in a beaker filled with DI water. The solution was sonicated using ultrasonic bath for 30 minutes. Then, the solution was transferred to the Schott bottle, where the ITO glass substrates were positioned at the bottom. Afterward, the bottle was immersed in water bath instrument for 2 h at temperature of 70ºC. After the immersion process, the ITO glass deposited with NiO films were taken out from the bottle and blown with nitrogen. Then, the samples were baked in a furnace for 10 min at 150ºC. The samples were annealed at diverse temperatures of 300 ºC, 400 ºC, 500 ºC. The process flow of the experiment is shown in Fig. 1.

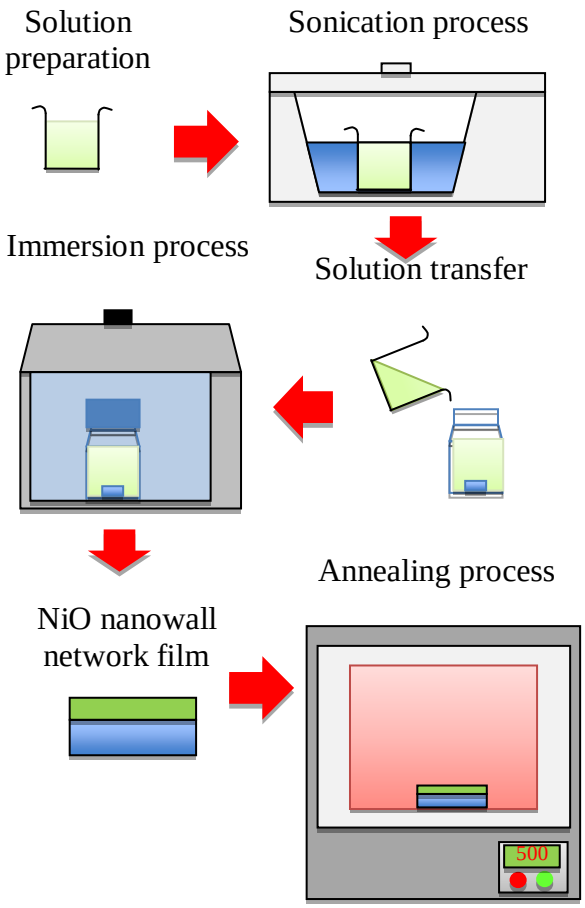

Fig. 1: The process flow to grow NiO nanowall network films using solution immersion method

Field-emission scanning electron microscopy (FESEM; JEOL JSM-7600F) was used to observe surface morphologies of the samples. The crystallinity properties of the samples were characterized by X-ray diffraction (XRD; PANalytical X'Pert PRO). The optical transmittance spectra of nanowall network films were characterized by ultraviolet-visible (UV-vis) spectroscopy (Jasco V-670). The humidity sensor measurements of the fabricated devices were performed using sensor measurement system (Keithley 2400) and humidity chamber (ESPEC-SH261). For humidity sensor measurement, gold (Au) contacts were deposited on top of the film by using thermal evaporation system (Ulvac VPC 1100). The thickness of the metal contact was fixed at 60nm. The humidity sensor structure using NiO nanowall network film is shown in Fig. 2.

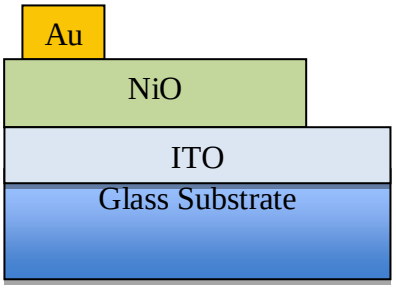

Fig. 2: The humidity sensor configuration using NiO nanowall network film

3. Results and Discussion

The FESEM surface morphology images of the as-deposited and annealed NiO films on ITO-coated glass substrates are shown in Fig. 3. The FESEM images are arranged according to the following sequence: a) as-deposited, b) 300 ^{0}C-annealed, c) 400 ^{0}C-annealed, and d) 500 ^{0}C-annealed NiO films. All films exhibit unique NiO nanowall network structures with high porous channel densities. As observed from the FESEM images, the nanowall arrays and porous channel structures for as-deposited, 300 ^{0}C-annealed, and 400 ^{0}C-annealed are nearly identical. These films reveals porous structure of well-connected particles to form nanowall networks. However, when the annealing temperature is increased to 500 ^{0}C, the nanowall structure deteriorated, where the presence of tiny black spots on the individual nanowall can be clearly observed in the FESEM image. The black spot represents void which originates from the evaporation of OH group and impurities that exist within the nanowall [27, 28]. The applied annealing temperature to the certain extent clearly plays important role in determining the structural behavior of the deposited NiO nanowall network films. In general, the high thermal energy from high annealing temperature provides sufficient kinetic energy to the system and enhances the reaction process inside the sample. As a result, the growth reaction process is enhanced, which increases the mobility of the atoms to move and subsequently, cause a merging activity of the NiO crystallites. These atoms tend to diffuse and rearrange themselves to achieve low surface energy by occupying the correct sites in the crystal lattice of NiO. Simultaneously, the OH groups and other impurities such as HMT evaporate at high temperature, which leave voids on the nanowall surfaces. These evaporation occurs dominantly at high temperature as manifested by the presence of small voids with high density on the nanowall surfaces for the sample annealed at 500 ^{0}C.

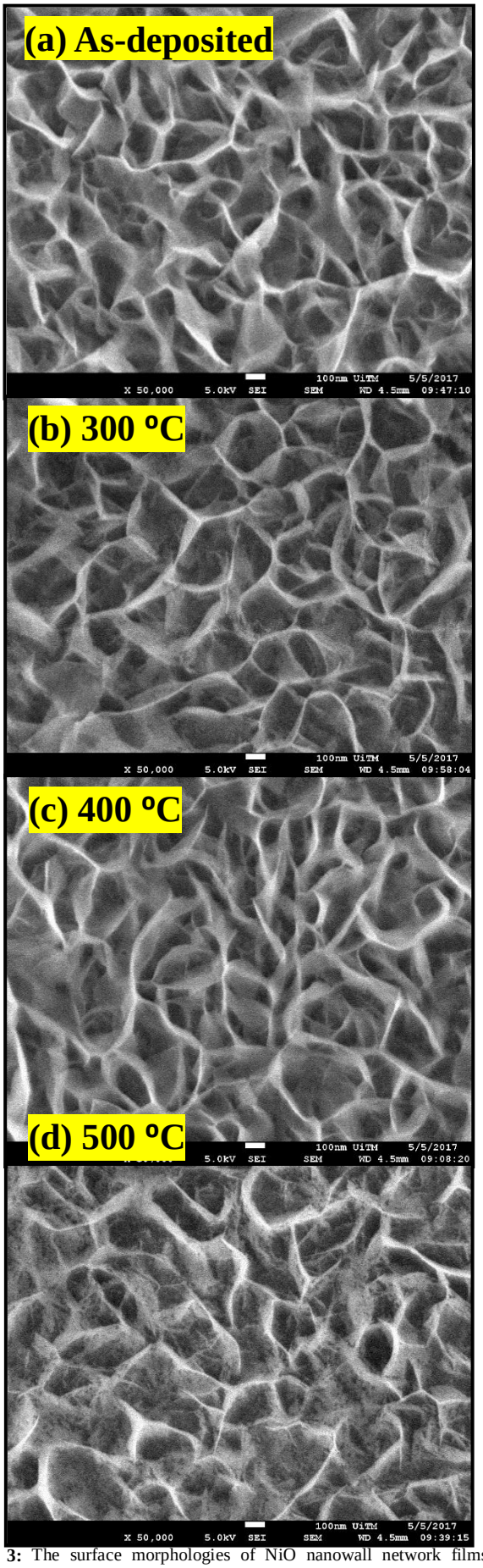

Fig. 3: The surface morphologies of NiO nanowall network films at different annealing temperatures

The XRD patterns for as-deposited and 500 ^{0}C-annealed NiO nanowall network films grown on ITO glass substrates are shown in Fig. 4. The XRD patterns indicate that both films display polycrystalline structure, which can be indexed to the cubic type of β-NiO (JCPDS NO.47-1049). The as-deposited and 500 ^{0}C-annealed NiO nanowall network films show diffraction peaks at approximately 37.9° and 43.8° corresponding to (111) and (200) crystal planes, respectively. Meanwhile, the diffraction peaks labelled with star belong to SnO_2 peaks from the ITO. The result shows that the as-deposited NiO film displays weaker intensity and broader peaks as compared with 500 ^{0}C-annealed film. This condition indicates that the crystallinity of as-deposited sample is poor and consists of amorphous structure. However, the XRD peaks for 500 ^{0}C-annealed film shows improved intensity, which implies that the crystallinity of the film is enhanced.

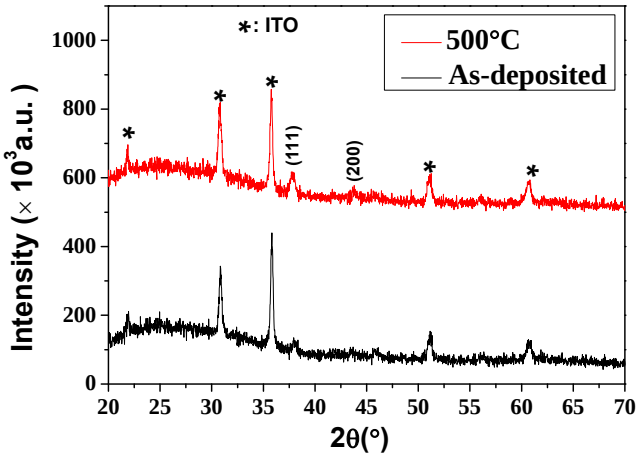

Fig. 4: The XRD patterns of as-deposited and 500 ^{0}C-annealed NiO nanowall network films

The transmittance spectra of NiO nanowall network films as a function of annealing temperatures are depicted in Fig. 5. All films have good transmittance properties in the visible region with the average transmittance values exceeding 90% at wavelength of 400-800 nm. The as-deposited, 300 ^{0}C-annealed, 400 ^{0}C-annealed, and 500 ^{0}C-annealed NiO nanowall network films have average transmittance of 94%, 92%, 90%, and 93%, respectively in the visible region (400-800 nm). The results suggested that the transmittance properties of NiO nanowall network films are almost constant regardless of annealing temperature. However, at wavelength below than 400 nm, the transmittance of all samples decrease. This result indicates that the NiO nanowall array films have good absorption properties in the UV region. To determine the optical bandgap of NiO nanowall array films, the Tauc's plot was constructed, which is based on the following equation:

$$(\alpha h\nu)^2 = A(h\nu - E_g) \quad (1)$$

where E_g, A, α, $h\nu$ is the optical bandgap, constant, absorption coefficient, and photon energy, respectively. The Tauc's plots of NiO nanowall network films at different annealing temperatures are presented in Fig. 6. The E_g of NiO nanowall network films at different annealing temperatures were determined from the extrapolated linear line of the graph of $(\alpha h\nu)^2$ versus *photon energy*. The estimated values are 3.77 eV, 3.77 eV, 3.76 eV, and 3.76 eV, for as-deposited, 300 ^{0}C-annealed, 400 ^{0}C-annealed, and 500 ^{0}C-annealed NiO nanowall network films, respectively. These results are in agreement with the reported bandgap values in the previous studies [29, 30].

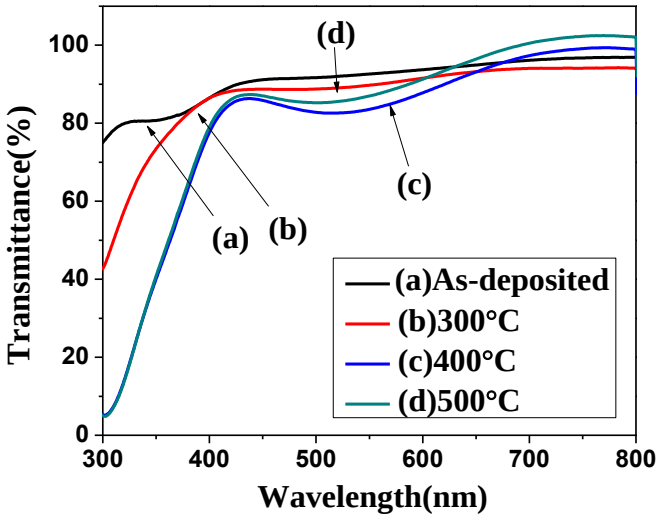

Fig. 5: The transmittance properties of NiO nanowall network films in the UV and visible regions

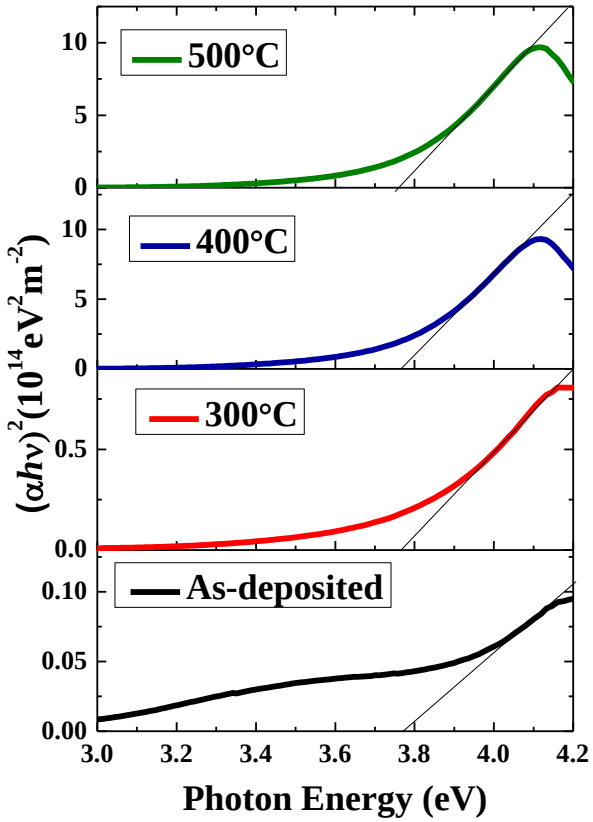

Fig. 6: The Tauc's plots of NiO nanowall network films for optical bandgap energy estimation

The change in the current signal of the as-deposited and annealed NiO nanowall network film-based humidity sensor devices for the various RH values is shown in Fig 7. The current signals of the samples were measured as a function of RH level at room temperature with the initial RH level was fixed at 40%RH. For this measurements, a 5 V bias was applied across the electrodes. From these measurements, all samples show increased current values with increasing RH values up to 90%RH. The as-deposited and 300 ^{0}C-annealed NiO nanowall network films show a smooth current response with exponent curve to the increased humidity. The current signal for 400 ^{0}C-annealed sample also shows exponent curve. However, the curve starts to show a slight deterioration at the increasing RH level. This deterioration in current signal is worse for 500 ^{0}C-annealed NiO nanowall network film. These results indicate that the humidity response for the sample annealed at high temperature is not stable. This condition might be due to the interchange of protonic to electronic conductions and vice-versa as suggested by Dhonge et al. [31]. When the NiO nanowall arrays annealed at high temperature, the crystal properties and purity of NiO improve, which enhance the p-type conductivity that NiO have natively. The enhancement of p-type conductivity might contribute to electronic conduction mechanism in the devices, which affect the current response at the increased RH level. Another possible reason is that the worsening structure of nanowall at high annealing temperature might play a role to distract the charge transportation in the sensor at the increased RH level. Further investigation need to be conducted in the future to verify this.

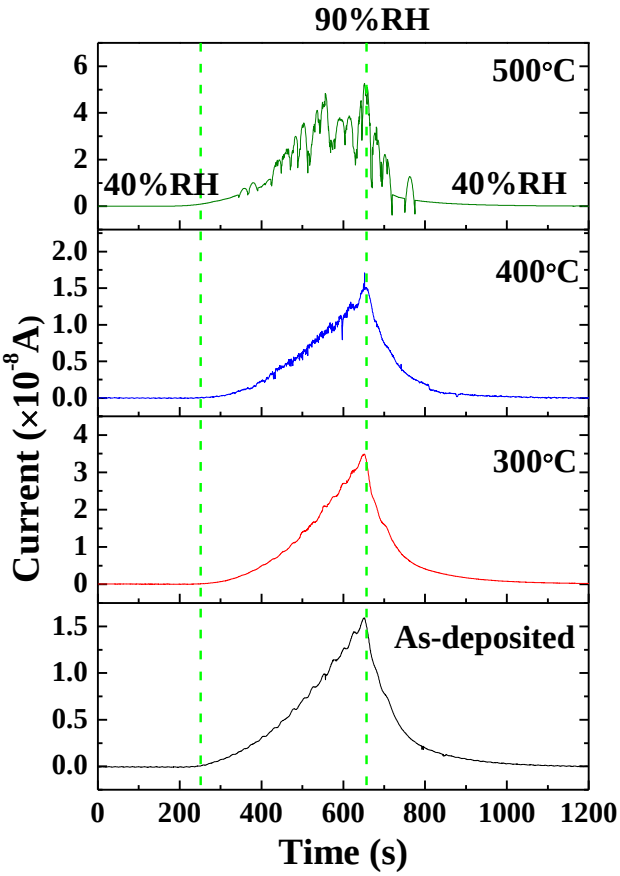

Fig. 7: The humidity sensing response of NiO nanowall network films annealed at different temperatures

From the humidity sensing plot, the sensitivity, S of the devices was estimated by using following equation:

$$S = \frac{I_{90}}{I_{40}} \quad (2)$$

where I_{90} and I_{40} is the current values at 90%RH and 40%RH, respectively. The sensitivity of NiO nanowall network films annealed at various temperature is shown in Fig. 8. The graph shows that the sensitivity of the device increases at high annealing temperature. The sensitivity values of the humidity sensor made from as-deposited, 300 ^{0}C-annealed, 400 ^{0}C-annealed, and 500 ^{0}C-annealed NiO nanowall network films are 4.36×10^2, 6.84×10^2, 6.71×10^2, and 1.80×10^3, respectively. The high sensitivity produced by NiO nanowall arrays annealed at high temperature in the ranges from 40%RH to 90%RH may be ascribed to the contribution of the high void density on nanowall surfaces and crystal improvement.

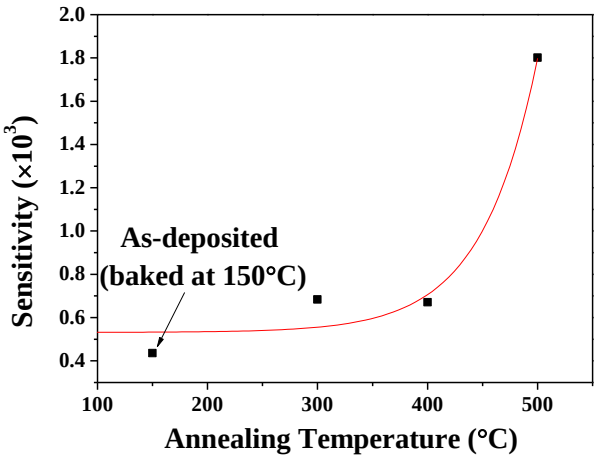

Fig. 8: The sensitivity plot of humidity sensor based on as-deposited and annealed NiO nanowall network films.

In general, the humidity sensing mechanism could be described as follows [10, 32, 33]. At low humidity level when the RH is increased slightly from initial humidity level of 40 %RH, the quantity of water molecules available is very small. The water molecules are adsorbed on the nanowall surface to form chemisorbed layer. The water molecules form chemisorbed monolayer on the nanowall surface by strong electrostatic interaction between Ni^{2+} and OH^-. This reaction leaves H^+ ions, which hop from one site to another site to contribute electric conduction. Thus, the current signal of the sensor increases at this stage due to the protonic conduction. When the humidity level increases, more water molecules are adsorbed on the nanowall surface. The adsorbed water molecules can form hydrogen bonds between themselves; that is between the chemisorbed OH^- layer and oxygen atom of water molecules via hydrogen bonding. As a result, physisorbed water layer is formed on top of chemisorbed water monolayer. Depending on the RH level, the thickness of physisorbed water layer will change. If the RH level is increased, the successive physisorbed water layer will stick on the first physisorbed water layer and the reaction process will be repeated to increase the thickness of physisorbed water layer. Thus, more H^+ ions are generated at high RH level to contribute more current signal in the process via protonic conduction. The H^+ ions can be generated from dissociation of hydronium ions at the physisorbed water layer as described by Grotthuss chain, as expressed:

$$2H_2O \rightarrow H_3O^+ + OH^- \quad (3)$$

$$H_3O^+ \rightarrow H_2O + H^+ \quad (4)$$

The protonic conduction occurs via proton hopping, which carries electric charge and happens along multiple series of hydrogen bonds between hydronium ions and water molecules. As the RH level increases, more charges are generated to contribute higher current signal. At very high humidity level, the large amount of water molecules adsorb between the nanowall networks to induce capillary condensation. During this stage, the charge transportation is significantly improved to produce more current signal in the process.

4. Conclusion

NiO nanowall network film were successfully prepared by sol-gel immersion method and annealed at different temperatures of 300 ^{0}C, 400 ^{0}C, and 500 ^{0}C. The structural, optical, and humidity sensing properties of the films were investigated. The FESEM images showed that the grown NiO films have nanowall network with porous channel structures. The NiO nanowall network film annealed at 500 ^{0}C showed deprivation in nanowall structure with the presence of high void density. The transmittance properties of NiO nanowall network films in the visible region are excellent with an average transmittance value above 90% for all samples. The humidity measurement results suggested that all samples were responsive to humidity level that ranges from 40%RH to 90%RH. The sensitivity of the sensors improved at high annealing temperature up to 500 ^{0}C. However, the stability of the curve was degraded for samples annealed at high annealing temperature.

Acknowledgement

The authors would like to acknowledge ASEAN-India Research & Training Fellowship (IMRC/AISTDF/R&D/P-1/2017) for the financial support. This work is also partially funded by REI grant (600-IRMI/REI 5/3 (017/2018)).The authors thank the Institute of Research Management and Innovation (IRMI) and Faculty of Electrical Engineering of UiTM for their support of this research.

References

[1] M. Gong, Y. Li, Y. Guo, X. Lv, X. Dou (2018), 2D TiO2 nanosheets for ultrasensitive humidity sensing application benefited by abundant surface oxygen vacancy defects, Sensors and Actuators B: Chemical 262, 350-358.

[2] W. Dong, Z. Ma, Q. Duan (2018), Preparation of stable crosslinked polyelectrolyte and the application for humidity sensing, Sensors and Actuators B: Chemical 272, 14-20.

[3] N.D.M. Sin, N. Samsudin, S. Ahmad, M.H. Mamat, M. Rusop (2013), Zn-Doped SnO2 with 3D Cubic Structure for Humidity Sensor, Procedia Engineering 56(0), 801-806.

[4] X. Ding, X. Chen, X. Chen, X. Zhao, N. Li (2018), A QCM humidity sensor based on fullerene/graphene oxide nanocomposites with high quality factor, Sensors and Actuators B: Chemical 266, 534-542.

[5] X. Leng, D. Luo, Z. Xu, F. Wang (2018), Modified graphene oxide/Nafion composite humidity sensor and its linear response to the relative humidity, Sensors and Actuators B: Chemical 257, 372-381.

[6] A.S. Ismail, M.H. Mamat, M.F. Malek, M.M. Yusoff, R. Mohamed, N.D.M. Sin, A.B. Suriani, M. Rusop (2018), Heterogeneous SnO2/ZnO nanoparticulate film: Facile synthesis and humidity sensing capability, Materials Science in Semiconductor Processing 81, 127-138.

[7] Y. Pang, J. Jian, T. Tu, Z. Yang, J. Ling, Y. Li, X. Wang, Y. Qiao, H. Tian, Y. Yang, T.-L. Ren (2018), Wearable humidity sensor based on porous graphene network for respiration monitoring, Biosensors and Bioelectronics 116, 123-129.

[8] M.H. Mamat, N.N. Hafizah, M. Rusop (2013), Fabrication of thin, dense and small-diameter zinc oxide nanorod array-based ultraviolet photoconductive sensors with high sensitivity by catalyst-free radio frequency magnetron sputtering, Materials Letters 93(0), 215-218.

[9] Y. Kumar, A. Sharma, Parasharam M. Shirage (2017), Shape-controlled CoFe2O4 nanoparticles as an excellent material for humidity sensing, RSC Advances 7(88), 55778-55785.

[10] S. Ismail, M.H. Mamat, N.D. Md. Sin, M.F. Malek, A.S. Zoolfakar, A.B. Suriani, A. Mohamed, M.K. Ahmad, M. Rusop (2016), Fabrication of hierarchical Sn-doped ZnO nanorod arrays through sonicated sol–gel immersion for room temperature, resistive-type humidity sensor applications, Ceramics International 42(8), 9785-9795.

[11] D. Zhang, D. Wang, X. Zong, G. Dong, Y. Zhang (2018), High-performance QCM humidity sensor based on graphene oxide/tin oxide/polyaniline ternary nanocomposite prepared by in-situ oxidative polymerization method, Sensors and Actuators B: Chemical 262, 531-541.

A. Gil, M. Fernández, I. Mendizábal, S.A. Korili, J. Soto-Armañanzas, A. Crespo-Durante, C. Gómez-Polo (2016), Fabrication of TiO2

coated metallic wires by the sol–gel technique as a humidity sensor, Ceramics International 42(7), 9292-9298.

[12] L. John Kennedy, P. Magesan, J. Judith Vijaya, M.J. Umapathy, U. Aruldoss (2014), Biominerals doped nanocrystalline nickel oxide as efficient humidity sensor: A green approach, Materials Science and Engineering: B 190, 13-20.

[13] M. Patel, H.-S. Kim, J. Kim, J.-H. Yun, S.J. Kim, E.H. Choi, H.-H. Park (2017), Excitonic metal oxide heterojunction (NiO/ZnO) solar cells for all-transparent module integration, Solar Energy Materials and Solar Cells 170, 246-253.

[14] R. Rajendran, Z. Yaakob, M.A. Mat Teridi, M.S. Abd Rahaman, K. Sopian (2014), Preparation of nanostructured p-NiO/n-Fe2O3 heterojunction and study of their enhanced photoelectrochemical water splitting performance, Materials Letters 133, 123-126.

[15] E. Turgut, Ö. Çoban, S. Sarıtaş, S. Tüzemen, M. Yıldırım, E. Gür (2018), Oxygen partial pressure effects on the RF sputtered p-type NiO hydrogen gas sensors, Applied Surface Science 435, 880-885.

[16] A.A. Ahmed, M. Devarajan, N. Afzal (2017), Effects of substrate temperature on the degradation of RF sputtered NiO properties, Materials Science in Semiconductor Processing 63, 137-141.

[17] M. Predanocy, I. Hotový, M. Čaplovičová (2017), Structural, optical and electrical properties of sputtered NiO thin films for gas detection, Applied Surface Science 395, 208-213.

[18] M. Ali, N. Remalli, V. Gedela, B. Padya, P.K. Jain, A. Al-Fatesh, U.A. Rana, V.V.S.S. Srikanth (2017), Ni nanoparticles prepared by simple chemical method for the synthesis of Ni/NiO-multi-layered graphene by chemical vapor deposition, Solid State Sciences 64, 34-40.

[19] N. Kaur, D. Zappa, M. Ferroni, N. Poli, M. Campanini, R. Negrea, E. Comini (2018), Branch-like NiO/ZnO heterostructures for VOC sensing, Sensors and Actuators B: Chemical 262, 477-485.

[20] D.R. Sahu, T.-J. Wu, S.-C. Wang, J.-L. Huang (2017), Electrochromic behavior of NiO film prepared by e-beam evaporation, Journal of Science: Advanced Materials and Devices 2(2), 225-232.

[21] S. Zhao, Y. Shen, P. Zhou, J. Zhang, W. Zhang, X. Chen, D. Wei, P. Fang, Y. Shen (2018), Highly selective NO2 sensor based on p-type nanocrystalline NiO thin films prepared by sol–gel dip coating, Ceramics International 44(1), 753-759.

[22] M.N. Siddique, A. Ahmed, P. Tripathi (2018), Electric transport and enhanced dielectric permittivity in pure and Al doped NiO nanostructures, Journal of Alloys and Compounds 735, 516-529.

[23] L.T. Hoa, H.N. Tien, S.H. Hur (2014), A highly sensitive UV sensor composed of 2D NiO nanosheets and 1D ZnO nanorods fabricated by a hydrothermal process, Sensors and Actuators A: Physical 207(0), 20-24.

[24] R. Lontio Fomekong, H.M. Tedjieukeng Kamta, J. Ngolui Lambi, D. Lahem, P. Eloy, M. Debliquy, A. Delcorte (2018), A sub-ppm level formaldehyde gas sensor based on Zn-doped NiO prepared by a co-precipitation route, Journal of Alloys and Compounds 731, 1188-1196.

[25] J. Song, L. Xu, R. Xing, W. Qin, Q. Dai, H. Song (2013), Ag nanoparticles coated NiO nanowires hierarchical nanocomposites electrode for nonenzymatic glucose biosensing, Sensors and Actuators B: Chemical 182, 675-681.

[26] M. H. Mamat, M.F. Malek, N.N. Hafizah, Z. Khusaimi, M.Z. Musa, M. Rusop (2014), Fabrication of an ultraviolet photoconductive sensor using novel nanostructured, nanohole-enhanced, aligned aluminium-doped zinc oxide nanorod arrays at low immersion times, Sensors and Actuators B: Chemical 195(0), 609-622.

[27] M.H. Mamat, M.I. Che Khalin, N.N.H. Nik Mohammad, Z. Khusaimi, N.D. Md Sin, S.S. Shariffudin, M. Mohamed Zahidi, M.R. Mahmood (2012), Effects of Annealing Environments on the Solution-Grown, Aligned Aluminium-Doped Zinc Oxide Nanorod-Array-Based Ultraviolet Photoconductive Sensor, Journal of Nanomaterials 2012, 189279.

[28] Y. Akaltun, T. Çayır (2015), Fabrication and characterization of NiO thin films prepared by SILAR method, Journal of Alloys and Compounds 625, 144-148.

[29] A.A. Akl, S.A. Mahmoud (2018), Effect of growth temperatures on the surface morphology, optical analysis, dielectric constants, electric susceptibility, Urbach and bandgap energy of sprayed NiO thin films, Optik 172, 783-793.

[30] B.P. Dhonge, S.S. Ray, B. Mwakikunga (2017), Electronic to protonic conduction switching in Cu2O nanostructured porous films: the effect of humidity exposure, RSC Advances 7(35), 21703-21712.

[31] S. Park, D. Lee, B. Kwak, H.-S. Lee, S. Lee, B. Yoo (2018), Synthesis of self-bridged ZnO nanowires and their humidity sensing properties, Sensors and Actuators B: Chemical 268, 293-298.

A. Sharma, Y. Kumar, K. Mazumder, A.K. Rana, P.M. Shirage (2018), Controlled Zn1−xNixO nanostructures for an excellent humidity sensor and a plausible sensing mechanism, New Journal of Chemistry 42(11), 8445-8457.